

# Interferometric Optical Gyroscope Based on an Integrated Si<sub>3</sub>N<sub>4</sub> Low-Loss Waveguide Coil

Sarat Gundavarapu<sup>1</sup>, Michael Belt, Taran A. Huffman<sup>1</sup>, Minh A. Tran<sup>1</sup>, *Student Member, IEEE*,  
Tin Komljenovic<sup>1</sup>, John E. Bowers<sup>1</sup>, *Fellow, IEEE, Fellow, OSA*,  
and Daniel J. Blumenthal, *Fellow, IEEE, Fellow, OSA*

**Abstract**—We describe the measurement and characterization of an interferometric optical gyroscope that uses an integrated 3-m large-area silicon nitride waveguide coil with waveguide loss <0.78 dB/m that is compatible with wafer-scale integration. The angle random walk and bias instability were measured to be 8.52°/h<sup>1/2</sup> and 58.7°/h, respectively. The measured performance is comparable to that of a commercial rate grade gyroscope, demonstrating that chip-scale integration is a feasible path to low cost, low power, compact implementation of optical gyroscope, and realization of longer coils will expand use of this technology to more demanding navigation applications.

**Index Terms**—Gyroscopes, inertial navigation, large area waveguide coils, optical sensors, ultra-low loss lithographic stitching.

## I. INTRODUCTION

**S**ENSORS used in the fields of guidance and navigation have been undergoing continuous development for more than six decades [1]. Advancements in gyroscope technologies have been instrumental in the realization of high precision inertial motion units (IMUs) and inertial navigation systems (INSs). While the accuracy and performance are important, many applications in navigation today require reduced size, cost, and operating power of the inertial sensor in addition to their accuracy [2]. Smaller sensors enable and impart guidance, navigation, and control into miniaturized, smart, self-guiding systems such as drones which were previously considered unrealizable. Based on their quality and performance, gyroscopes are categorized in to different grades as listed in Table I. Microelectromechanical (MEMS) gyroscopes, ring laser gyroscopes (RLGs), and interferometric fiber optic gyroscopes (IFOGs) are among the

Manuscript received August 18, 2017; revised September 13, 2017; accepted September 30, 2017. Date of publication October 22, 2017; date of current version February 24, 2018. This work was supported by Defense Advance Research Project Agency Office of Microsystems Technology (DARPA/MTO) under iWOG contract No: HR0011-14-C-0111. The views and conclusions contained in this document are those of the authors and should not be interpreted as representing official policies of DARPA or the U.S. Government. (*Corresponding author: Sarat Gundavarapu.*)

S. Gundavarapu, T. A. Huffman, M. A. Tran, T. Komljenovic, J. E. Bowers, and D. J. Blumenthal are with the Department of Electrical and Computer Engineering, University of California, Santa Barbara, CA 93106 USA (e-mail: saratchandra@ece.ucsb.edu; thuffman@ece.ucsb.edu; minhtran@ece.ucsb.edu; tin.komljenovic@gmail.com; bowers@ece.ucsb.edu; danb@ece.ucsb.edu).

M. Belt is with Honeywell International, Inc., Broomfield, CO 80021 USA (e-mail: Michael.Belt@honeywell.com).

Color versions of one or more of the figures in this paper are available online at <http://ieeexplore.ieee.org>.

Digital Object Identifier 10.1109/JLT.2017.2765918

TABLE I  
CLASSIFICATION OF GYROSCOPES BY PERFORMANCE [4]

Type	Angle random walk (deg/√hr)	Bias instability (deg/hr)
Rate grade (this work)	> 0.5	10 to 1000
Tactical grade	0.5 to 0.05	1 to 10
Intermediate grade	0.05 to 0.005	0.01 to 1
Inertial grade	< 0.005	< 0.01
Strategic grade	< 0.0003	< 0.001

commercially mature and available technologies today that are widely used in navigation, tactical, and industrial applications.

While optical gyroscopes have traditionally been expensive, their decreased vibrational sensitivity and rate random walk makes them superior to their MEMS counterparts. Accordingly, MEMS sensors are widely used in commercial and rate grade sensor applications requiring lower sensitivity at reduced cost and RLGs are employed as tactical and navigation grade sensors in IMUs [3]. Based on the design and performance, IFOGs can range from low cost, smaller area industrial rate grade sensors to expensive large area strategic or precision grade devices to be used in IMU/INS systems [4]. This versatility has attracted considerable research in the size reduction of interferometric optical gyroscopes (IOGs) while maintaining their high sensitivity and performance specifications. However, the cost and complexity of assembling high quality fiber optic based gyroscopes requiring precision alignment and assembly of discrete optical components, and sensitivity to manufacturing and environmental variations has led to an increased need to integrate them at the chip-scale.

The performance of an IOG improves with increased enclosed area and is degraded by the limited polarization extinction of the optical coils. Chip scale integration can improve the manufacturability of IOGs in general, while at the same time addressing polarization misalignment issues and significantly reducing the size, weight, and cost. It has been challenging to realize an on-chip waveguide coil based IOG with desired performance due to the absence of an integration platform that realizes very low waveguide loss over the required large on-chip coil lengths, a high degree of polarization selectivity and integration with other key elements like fiber to waveguide mode transformers and low loss waveguide crossings. The Si<sub>3</sub>N<sub>4</sub> based ultra-low loss waveguide (ULLW) platform [4], [5] provides a wafer-

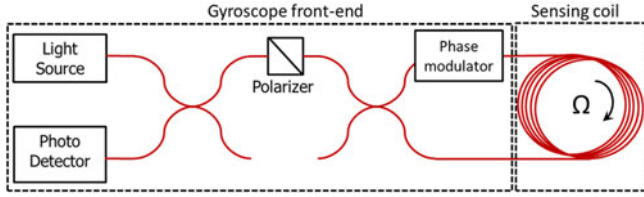


Fig. 1. Minimum reciprocal configuration of an IFOG (polarizer being an optional component). Physical dimensions and type of the sensing coil is varied based on the targeted application of sensor.

scale compatible solution to enable long, on-chip waveguide coils with losses as low as 0.1 dB/m [5]. In addition to the low waveguide loss and high polarization dependent loss ( $>75$  dB) of ULLW  $\text{Si}_3\text{N}_4$  coils [7], the low nonlinear loss and high non-linearity thresholds (compared to other waveguide platforms) [8], play an important role in minimizing parasitic effects due to the optical Kerr effect, and non-reciprocal polarization drift normally associated with using bulk optical components, thus resulting in improved gyroscope performance. A chip scale IOG can be achieved by three dimensional close-packed multi-chip integration of waveguide coil and integrated front-end chips. A fully integrated IOG can be realized by integrating the gyroscope front-end and low loss waveguide coil onto a single chip thereby exploiting the passive and active function of integrated front ends with the low loss of  $\text{Si}_3\text{N}_4$  coils. The  $\text{Si}_3\text{N}_4$  waveguide coil based gyroscope with active optical components on a heterogeneously integrated III/V-Silicon platform has been proposed and analyzed in [9]. Detailed design and characterization of integrated optical components for a IOG are presented in [10]. We reported the preliminary results of a Sagnac sensor realized using this ultra-low loss high aspect ratio  $\text{Si}_3\text{N}_4/\text{SiO}_2$  planar waveguide coil in our previous work [11].

This paper is an extended version of our submission to OFS- 25 which can be found at [12]. In this paper, we present a more detailed view of design and characterization of low loss integrated waveguide coil based gyroscope. We also discuss two approaches to integrate the optical active components with waveguide coil to realize an on-chip gyroscope sensor. We begin with the general setup for an IFOG in Section II followed by the design, fabrication, and packaging of waveguide coil in Section III. Section IV discusses the rotation rate measurements and noise characterization of gyroscope. The prospects for full integration and improvements in gyroscope performance using a longer coil with lower packaging losses are discussed in Section V followed by the summary and conclusion of the work.

## II. OVERVIEW OF DESIGN AND PERFORMANCE OF IOG

The interferometric optical gyro operates on the principle of Sagnac phase shift [4]. The Sagnac phase shift  $\Delta\Phi_R$  induced due to rotation in an IOG about the axis with rate  $\Omega$ , as illustrated in Fig. 1, is given by

$$\Delta\Phi_R = \left( \frac{8\pi}{c \cdot \lambda} \right) \cdot A_{\text{enc}} \cdot \Omega \quad (1)$$

$$A_{\text{enc}} = N \cdot A \quad (2)$$

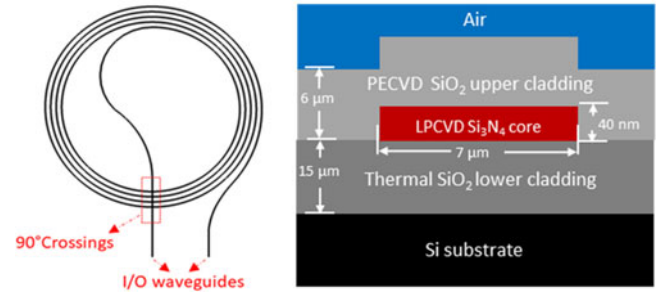


Fig. 2. (Left) Illustration of Archimedian waveguide spiral for an IOG. (Right) Cross section of ULLW structure with 40-nm core to achieve lowest propagation loss.

where  $A_{\text{enc}}$  is the area enclosed in the sensing coil,  $\lambda$  is the mean wavelength of the optical source, and  $\Omega$  is the rotation rate. For an IFOG, area enclosed is the sum of areas of each turn of the fiber sensing coil as shown in (2), where  $N$  is the number of turns and  $A$  is area enclosed by an individual turn of the coil.

The performance for a given enclosed area of sensing coil of an IOG is limited by the propagation loss and intrinsic noise sources that affect the performance including detected thermal noise and shot noise, laser relative intensity noise and un-desired interferometric effects that interfere with the desired detected signal, such as coherent backscattering and reflections, the optical Kerr effect, and polarization non-reciprocities [9]. The phase shift induced by these non-reciprocities degrades the angle random walk and bias instability of the IOG. To address non-reciprocal polarization effects, polarization maintaining (PM) fiber and components can be employed, however the net polarization bias error is limited by the polarization extinction ratio (PER) of the sensing coil, the intensity rejection ratio of the polarizer and manufacturing and environment polarization misalignment and induced polarization coupling.

The RMS value of polarization bias error  $\sigma_{\Delta\varphi_e}$  induced by a sensing coil of length,  $L$ , mean rate of power transfer between the polarization modes  $h$  ( $\text{PER} = h \cdot L$ ), depolarization length  $L_d$ , and intensity rejection ratio of polarizer  $\epsilon^2$  is given by [4]

$$\sigma_{\Delta\varphi_e} = \frac{\epsilon^2 h L}{\sqrt{N}} \quad (3)$$

where  $N = L/L_d$  is the number of depolarization lengths. While the typical  $\epsilon^2$  of a fiber polarizer is limited to around 25–30 dB, high aspect ratio 40-nm core  $\text{Si}_3\text{N}_4$  waveguides have been shown to have PERs  $>75$  dB [7], indicating a suppression of the polarization bias error by more than 4 orders of magnitude.

## III. INTEGRATED GYROSCOPE

### A. Integrated Coil Design and Fabrication

The design goal for waveguide coil to be used in an IOG is to realize largest possible area of coil with lowest possible attenuation. This translates to choosing an optimal length for a given waveguide loss to meet the required area and hence, desired gyroscope sensitivity. Archimedian spirals as shown in Fig. 2, are ideal geometry to achieve maximum enclosed

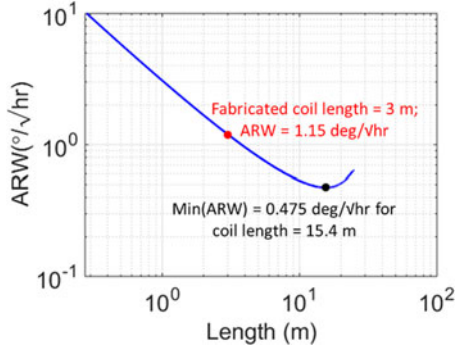


Fig. 3. Estimation of angle random walk for varying coil length.

area and length for a given chip footprint. For an Archimedean spiral defined by  $\rho = a + b\theta$ , where  $a$  is the minimum radius and  $b = \frac{1}{2\pi} \times$  turn radius difference, and  $N$  turns, the effective enclosed area is given by

$$\begin{aligned} A_{\text{enc}} &= \iint \rho \, d\rho \, d\theta = \frac{1}{2} \int_0^{2N\pi} \rho^2 \, d\theta \\ &= N\pi \left[ a^2 + \frac{b^2}{3} (2N\pi)^2 + 2N\pi ab \right] \end{aligned} \quad (4)$$

The use of thinner waveguide cores improves propagation and crossing losses (assuming operating in the region where sidewall roughness is the dominant contribution to both these characteristics) but places a limitation on the minimum waveguide bend radius [5]. Here we choose a waveguide structure with 40-nm thick Si<sub>3</sub>N<sub>4</sub> core, shown in Fig. 2 to give us minimal possible loss values, which constrains our bend radius to 11 mm. The lithographic stepper system ASML PAS 5500 DUV used in our fabrication process has a maximum die size of 21 × 25 mm that limited the bend radius to 10 mm within a single field. To overcome the limitation of die size of our DUV stepper and to realize a large area coil, we used ultra-low loss stitching [13] of 4 different DUV fields which increased the achievable coil radius to 20 mm.

Using (4) and the approach described in [9], the optimal length of the ULLW Si<sub>3</sub>N<sub>4</sub> coil to be used in an integrated optical gyroscope to achieve ARW close to 1 deg/√hr was estimated as shown in Fig. 3 to be about 3–10 m. The simulated value accounts for an excess packaging loss of 1 dB/m, RIN of −128 dBc/Hz and waveguide loss of 0.8 dB/m using an optical input power of 100 mW. The estimated ARW of IOG with a 3-m integrated waveguide coil used in this paper, as shown in Fig. 3, is close to 1.15 deg/√hr.

The design parameters for fabricating the waveguide coil with 40 nm × 7 μm waveguide coil used in this paper are summarized in Table II. Fabricated coil and crossing structures are shown in Fig. 4.

Waveguide loss of the coil was characterized using optical backscattering reflectometry (OBR). Different loss sources contributing to the total loss of the waveguide coil are listed in Table III. Complete details about the large area waveguide coil design and characterization can be found in [13], [14].

TABLE II  
SUMMARY OF WAVEGUIDE COIL DESIGN PARAMETERS

	Value
Coil length	3 m
Outer radius	20 mm
Inner radius	17.25 mm
Waveguide spacing	50 μm
Number of crossings	50
Enclosed area	278 cm <sup>2</sup>
Estimated ARW	1.15 deg/√hr

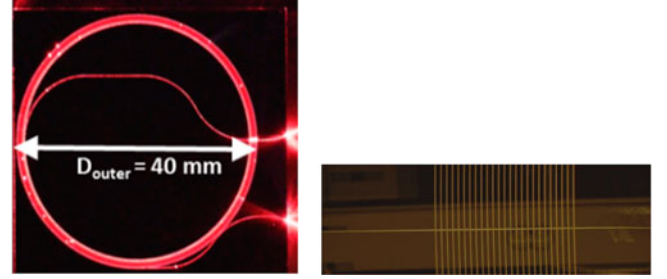


Fig. 4. (Left) Top view of fabricated 3 m waveguide coil illuminated using a red laser. (Right) Dark field optical image of 90° crossings of the fabricated spiral.

TABLE III  
SUMMARY OF LOSS CONTRIBUTIONS IN WAVEGUIDE COIL [14]

	Value
Waveguide and stitching loss*	0.78 dB/m
Crossing loss	0.0156 dB/crossing

\* indicates the minimum waveguide and stitching loss measured at 1595 nm. At 1550 nm, waveguide loss is close to 1.5 dB/m. Estimated ARW for a waveguide loss of 1.5 dB/m, measured RIN of −122 dBc/Hz, and an excess packaging loss of 12 dB was around 2.23 deg/√hr.

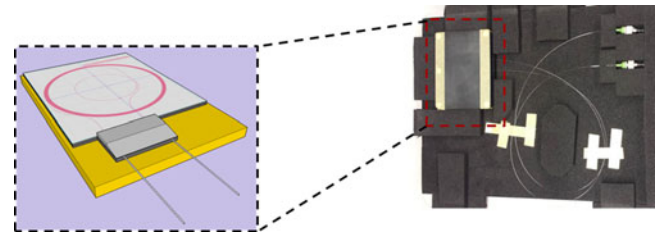


Fig. 5. (Left) Illustration of the 3-m Si<sub>3</sub>N<sub>4</sub> waveguide coil edge coupled to PM fibers using a VGA. (Right) Actual packaged coil with FC/APC connectors (used to minimize reflections).

### B. Packaged Coil

To assess the performance of waveguide coil as the sensing element in a gyroscope, we packaged the coil and mounted it on a rotation stage for measurements. In order to reduce the polarization induced drift and to improve stability of device packaging, a custom-made V-groove array (VGA) was used to house polarization maintaining fibers which were edge coupled to Si<sub>3</sub>N<sub>4</sub> waveguides as shown in Fig. 5. Dymax epoxies OP-54 and

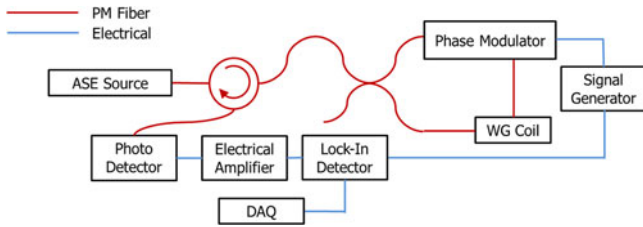


Fig. 6. Setup for characterization of gyroscope based on a waveguide (WG) coil. SRS 844 lock-in was used for demodulation and a National instruments (NI) data acquisition (DAQ) was used to collect the output data.

OP-67-LS were used to put the VGA in place after alignment followed by a UV curing procedure using Dymax Bluewave 75 to bond the VGA to the plate. The mode mismatch between highly elliptical mode of our untapered waveguide and nearly circular mode of the fiber resulted in increase of fiber-chip coupling loss. In addition, the drift of the fibers post UV cure increased the coupling loss further, causing a total loss of >6 dB per facet, resulting in a total insertion loss for the waveguide coil to be 16.2 dB with a broadband source for the packaged device.

#### IV. GYROSCOPE CHARACTERIZATION AND PERFORMANCE MEASUREMENTS

##### A. Proper Frequency

The rotation rate output of an IOG is evaluated using the amplitude of first harmonic of bias modulation frequency in the output of the reflected signal. To achieve perfect rejection of all the even harmonics, realize maximum sensitivity, and suppress other parasitic noise sources, the bias modulation should be at a frequency  $f_p$ , which is the inverse of twice the transit delay,  $\Delta\tau_g$  of the sensing coil.

$$f_p = \frac{1}{2 \cdot \Delta\tau_g} \quad (5)$$

This frequency is known as the proper (eigen) frequency [4], [11], [12] of the coil where the gyroscope operates with maximum sensitivity. We utilized square wave biasing scheme to further suppress the spurious effects due to nonlinear response of modulator [4]. The gyroscope characterization was performed using an in-house assembled setup is shown in Fig. 6. Two 20 dB ZFL-1000LN RF amplifiers were cascaded between the photo detector and the lock-in amplifier to improve the signal to noise ratio. The time constant and filter slope for demodulation using lock-in were set to 300 ms and 24 dB/octave respectively.

The proper frequency of our waveguide coil gyroscope, determined by performing a ramp frequency sweep (as described in our previous paper [11]), was found to be 21.02 MHz (shown in Fig. 7.). The measured value agrees well with the expected value of proper frequency based on actual length of the sensing coil (3 m waveguide coil + fiber pig tails  $\sim$ 5 m).

##### B. Rotation Signal Measurement and Noise Characterization

To correlate the measured output value of gyroscope to the input rotation rate, we placed the setup on a calibrated rotation

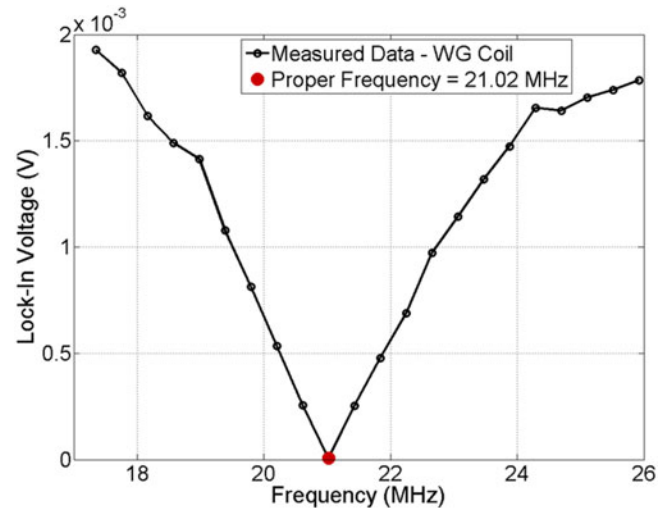


Fig. 7. Measured proper frequency of the sensing coil with 3-m  $\text{Si}_3\text{N}_4$  waveguide in the loop and about 2-m PM fiber pig tails.

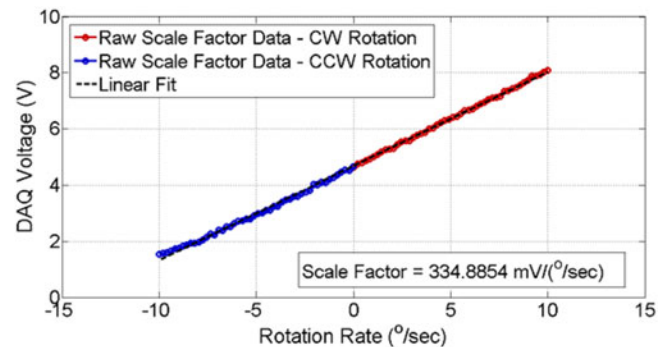


Fig. 8. Measured output was quite linear with the input rotation rate and the difference in scale factor between CW and CCW rotation rates was very small.

stage and measured the scale factor of the sensor. To accomplish this, we used a high precision rotation stage (Ideal Aeromsmith 1270VS) and the applied rotation rate was swept from 0.02 deg/sec to 10 deg/sec in both CW and CCW directions. The scale factor was measured to be approximately 335 mV/deg/sec, as shown in Fig. 8.

The detection limit of the gyroscope was characterized with the setup at rest using the standard Allan deviation technique [15]. The samples were captured using NI-DAQ at a rate of 50 Hz for an hour. The plot of Allan variance for one hour of data is shown in Fig. 9. A  $-0.5$ -slope line was fit to the data to extract the angle random walk or the detection limit of the system to be 8.52 deg/ $\sqrt{\text{hr}}$ . The bias instability of the gyroscope is evaluated from the flat portion (slope = 0) of the Allan deviation plot. As seen in, there is a flat portion (A) at 0.03 hr which gives a BIS of 58.68 deg/hr and another flat portion (B) at around 0.1 hr, which yields a BIS of 45.42 deg/hr before noise becomes predominantly rate random walk (slope = 1).

To further verify the value of bias instability, we performed an Allan deviation measurement for five hours at a sample rate of 10 Hz and lock-in time constant of 3 s. The flat portion on this Allan deviation plot was observed at 0.034 hr as shown in Fig. 10 yielding a BIS of 68.4 deg/hr which is closer to the

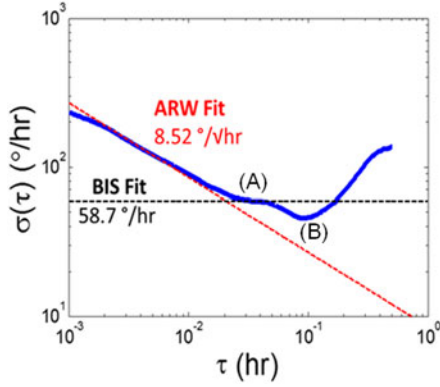


Fig. 9. Allan deviation measurement with lock-in time constant of 300 ms, with a filter slope of 24 dB/octave and a sampling rate of 50 Hz.

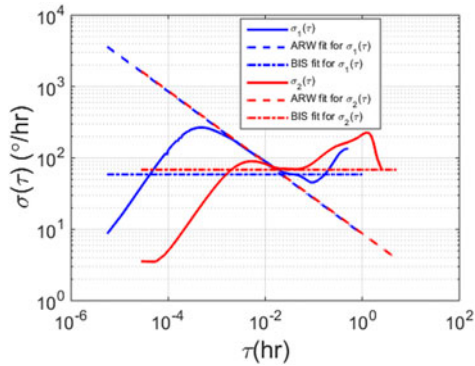


Fig. 10.  $\sigma_1(\tau)$  and  $\sigma_2(\tau)$  refer to the Allan deviation measurements with time constant of 300 ms and 3 s, respectively; Allan deviation is valid only from  $\tau = (1/\text{ENBW})$  s.

TABLE IV  
SUMMARY OF MEASUREMENTS

$\tau_{\text{int}}$ (ms)	ENBW (Hz)	SF (V/deg/sec)	ARW (deg/ $\sqrt{\text{hr}}$ )	BIS (deg/hr)	$f_{\text{sam}}$ (Hz)
300	0.26	0.335	8.52	58.68	50
3	0.026	0.33	8.7	68.4	10

$\tau_{\text{int}}$  = Lock-in time constant; ENBW = Effective noise bandwidth for filter slope of 24 dB/oct; SF = scale factor;  $f_{\text{sam}}$  is the DAQ sampling rate; ENBW =  $(5/64\tau_{\text{int}})$  for a filter slope of 24 dB/oct.

58.68 deg/hr measured in region (A) of Fig. 9. High value of bias instability suggests that  $1/f$  flicker noise from electrical components to be the dominant noise source. Summary of all gyroscope measurements is given in Table IV.

## V. PROSPECTS FOR FULL INTEGRATION AND PACKAGING

Integration of active optical components along with the waveguide coil will help us realize a chip scale version of IOG.

While broadband sources are the preferred optical sources for most of the commercial IFOGs because of their immunity to several noise sources of gyro such as coherent backscattering [4], use of a laser that is spectrally broadened with direct [16]–[19] or external [20], [21] frequency/phase modulation has attracted considerable attention in the recent years. Because of their advantages such as smaller footprint, higher power efficiency, and higher wavelength stability (that translates to higher scale factor stability), a frequency modulated (FM) laser will be a more

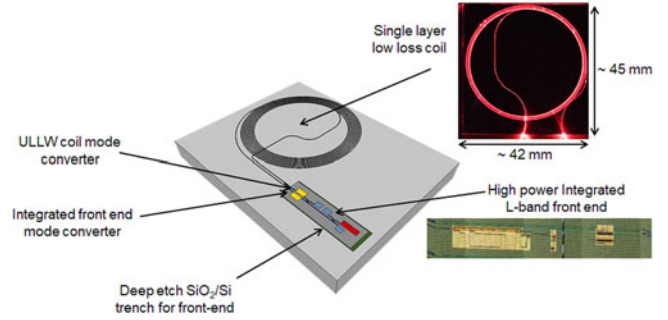


Fig. 11. Schematic of the proposed fully multichip IOG with integrated front-end chip placed in a deep-etch SiO<sub>2</sub>/Si trench on the waveguide coil chip. Mode converters on both the chips help in realizing smaller coupling losses.

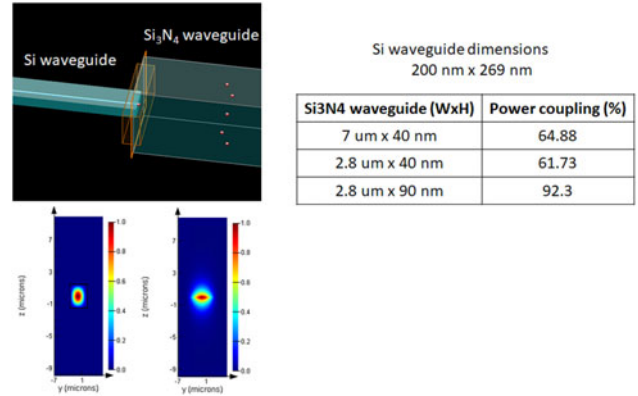


Fig. 12. Example design of mode converters (using mode solutions in Lumerical [22]) between Si<sub>3</sub>N<sub>4</sub> and Si waveguides showing the power coupling efficiency for different geometries of Si<sub>3</sub>N<sub>4</sub> waveguide.

suitable candidate for a chip scale gyroscope. An integrated photonic chip with an optical source, two couplers, three photodiodes, and two phase modulators within an area of 4.5 mm<sup>2</sup> that can be used to realize a chip scale gyroscope was demonstrated by the authors, details of which can be found in [10].

Multi-chip photonic integration of the low loss waveguide coil and integrated front-end chip can be used to realize a chip scale IOG. The integrated front-end chip can be placed in a deep-etch cavity on the waveguide coil chip, aligned and epoxied to realize a hybrid chip version of IOG as shown in Fig. 11.

With customized tapers designed for both Si<sub>3</sub>N<sub>4</sub> and Si waveguides as shown in Fig. 12, the low loss waveguide coil can be coupled with the integrated front-end with minimal coupling losses.

A fully integrated waveguide coil based gyroscope can be realized using vertical coupling between Si<sub>3</sub>N<sub>4</sub> and Si waveguide layers. Such coupling can be used to integrate Si<sub>3</sub>N<sub>4</sub> waveguide coil with the integrated front-end. Coupling losses of  $(0.4 \pm 0.2)$  dB per transition between silicon and ULLW layers have been demonstrated in [23] that would provide a solution to alleviate the high fiber to waveguide coupling loss through seamless chip scale integration of all IOG components (III–V/Si actives with ULL Si<sub>3</sub>N<sub>4</sub> coils) and realize a fully integrated waveguide coil based interferometric optical gyroscope as shown in Fig. 13. The phase modulator is operated in push-pull configuration using two electrodes (yellow) to reduce driving voltage and jitter improving the power efficiency and performance of the sensor.

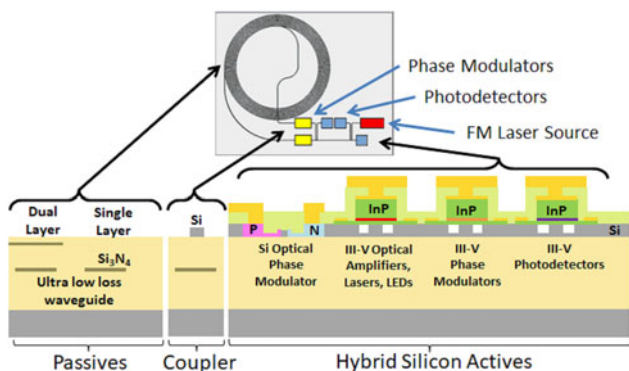


Fig. 13. Schematic of proposed fully integrated optical waveguide gyroscope with a ULLW coil in  $\text{Si}_3\text{N}_4$  with heterogeneous III/V-Si front-end.

## VI. CONCLUSION

We reported the rotation rate measurements of an interferometric optical gyroscope using an ultra-low loss  $\text{Si}_3\text{N}_4$  waveguide coil. The measured gyroscope sensitivity ( $\text{ARW} = 8.52 \text{ deg}/\sqrt{\text{hr}}$ ) was found to be in the same order as that of a commercial rate grade sensor. Reduction of flicker noise by using low noise electrical components and decrease in the total packaging loss to less than 1 dB (currently 12 dB) will greatly improve the performance of gyroscope and bridge the mismatch between values of measured and simulated sensitivity. We estimated that the ARW can be reduced to  $0.52 \text{ deg}/\sqrt{\text{hr}}$  for the current 3 m coil by decreasing the RIN of optical source from  $-128 \text{ dBc/Hz}$  to  $-140 \text{ dBc/Hz}$ . This suggests that use of a frequency/phase modulated laser source, because of its low RIN, can result in significantly better gyroscope performance. Simulations in [13], [14] show that further improvements in waveguide losses and increase in the waveguide coil length (15 m) using a broadband source with 100 mW of optical power having a RIN of  $-128 \text{ dBc/Hz}$  will push the sensitivity down to that of a tactical grade sensor ( $\text{ARW} = 0.475 \text{ deg}/\sqrt{\text{hr}}$ ). Reduction in waveguide propagation loss enables realization of larger area coils that can further improve the performance of the sensor. In conclusion, results show that ultra-low loss waveguide coils offer a promising solution to realize a fully integrated waveguide optical gyroscope (IWOG) as shown in Fig. 13 that is resilient to several noise factors such as errors related to optical non-linearities and polarization drift.

## ACKNOWLEDGMENT

The authors would like to thank Robert Lutwak and Michael Davenport for useful discussions.

## REFERENCES

- [1] A. D. King, "Inertial navigation—Forty years of evolution," *GEC Rev.*, vol. 13, no. 3, pp. 140–149, 1998.
- [2] N. Barbour, "Inertial navigation sensors," *NATO RTO Lecture Ser.*, vol. 116, pp. 1–24, 2004.
- [3] G. A. Sanders *et al.*, "Fiber optic gyro development at Honeywell," *Proc. SPIE*, vol. 9852, 2016, Art. no. 985207.
- [4] H. C. Lefevre, *The Fiber-Optic Gyroscope*, 2nd ed. Norwood, MA, USA: Artech House, 2014.

- [5] J. F. Bauters *et al.*, "Planar waveguides with less than 0.1 dB/m propagation loss fabricated with wafer bonding," *Opt. Express*, vol. 19, no. 24, pp. 24090–24101, 2011.
- [6] A. Leinse, S. Zhang, and R. Heideman, "TriPleX: The versatile silicon nitride waveguide platform," in *Proc. Prog. Electromagn. Res. Symp.*, 2016, pp. 67–67.
- [7] J. F. Bauters, M. J. R. Heck, D. Dai, J. S. Barton, D. J. Blumenthal, and J. E. Bowers, "Ultralow-loss planar  $\text{Si}_3\text{N}_4$  waveguide polarizers," *IEEE Photon. J.*, vol. 5, no. 1, Feb. 2013, Art. no. 6600207.
- [8] M.-C. Tien, J. F. Bauters, M. J. R. Heck, D. J. Blumenthal, and J. E. Bowers, "Ultra-low loss  $\text{Si}_3\text{N}_4$  waveguides with low nonlinearity and high power handling capability," *Opt. Express*, vol. 18, no. 23, pp. 23562–23568, 2010.
- [9] S. Srinivasan, R. Moreira, D. Blumenthal, and J. E. Bowers, "Design of integrated hybrid silicon waveguide optical gyroscope," *Opt. Express*, vol. 22, no. 21, pp. 24988–24993, 2014.
- [10] M. A. Tran *et al.*, "Integrated optical driver for interferometric optical gyroscopes," *Opt. Express*, vol. 4, no. 4, pp. 3826–3840, 2017.
- [11] S. Gundavarapu, T. Huffman, R. Moreira, M. Belt, J. E. Bowers, and J. Daniel, "Integrated ultra-low-loss silicon nitride waveguide coil for optical gyroscopes," in *Proc. Opt. Fiber Commun. Conf.*, 2016, vol. 1, pp. 4–6.
- [12] S. Gundavarapu *et al.*, "Integrated Sagnac optical gyroscope sensor using ultra-low loss high aspect ratio silicon nitride waveguide coil," *Proc. SPIE*, vol. 10323, 2017, Art. no. 103231A.
- [13] T. Huffman, M. Davenport, M. Belt, J. E. Bowers, and D. J. Blumenthal, "Ultra-low loss stitching for large-area waveguide based delay-line gyroscopes," in *Proc. IEEE Photon. Conf.*, 2016, pp. 478–479.
- [14] T. Huffman, M. Davenport, M. Belt, J. E. Bowers, and D. J. Blumenthal, "Ultra-low loss large area waveguide coils for integrated optical gyroscopes," *IEEE Photon. Technol. Lett.*, vol. 29, no. 2, pp. 185–188, Jan. 15, 2017.
- [15] *IEEE Standard Specification Format Guide and Test Procedure for Single-Axis Interferometric Fiber Optic Gyros*, IEEE Standard 952-1997, 1998.
- [16] T. Komljenovic *et al.*, "Frequency modulated lasers for interferometric optical gyroscopes," *Opt. Lett.*, vol. 41, no. 8, pp. 1773–1776, 2016.
- [17] S. Gundavarapu *et al.*, "Effect of direct PRBS modulation on laser driven fiber optic gyroscope," in *Proc. IEEE Int. Symp. Inertial Sens. Syst.*, 2017, vol. 1, pp. 1–3.
- [18] M. A. Tran *et al.*, "Frequency modulated laser based interferometric optical gyroscope," in *Proc. Conf. Lasers Electro-Opt.*, 2016, Paper JTu5A.140.
- [19] J. E. Shen *et al.*, "Frequency modulated laser optical gyroscope," in *Proc. IEEE Photon. Conf.*, 2015, pp. 431–432.
- [20] J. Chamoun and M. J. F. Digonnet, "Aircraft-navigation-grade laser-driven FOG with Gaussian-noise phase modulation," *Opt. Lett.*, vol. 42, no. 8, pp. 1600–1603, 2017.
- [21] M. J. F. Digonnet and J. N. Chamoun, "Recent developments in laser-driven and hollow-core fiber optic gyroscopes," *Proc. SPIE*, vol. 9852, 2016, Art. no. 985204.
- [22] M. Papes *et al.*, "Fiber-chip edge coupler with large mode size for silicon photonic wire waveguides," *Opt. Express*, vol. 24, no. 5, pp. 5026–5038, 2016.
- [23] J. F. Bauters *et al.*, "Silicon on ultra-low-loss waveguide photonic integration platform," *Opt. Express*, vol. 21, no. 1, pp. 544–555, 2013.

**Sarat Gundavarapu** received the bachelor's degree in electronics and communication engineering from Jawaharlal Nehru Technological University, Hyderabad, India, in 2007. He is currently working toward the Ph.D. degree in electrical engineering with the University of California, Santa Barbara, CA, USA. His research interests include silicon nitride photonics and optical sensors.

**Michael Belt** received the B.S. degree in electrical and computer engineering from The Ohio State University, Columbus, OH, USA, in 2010, and the M.S. and Ph.D. degrees in electrical engineering from the University of California, Santa Barbara (UCSB), Santa Barbara, CA, USA, in 2012 and 2017, respectively.

He is currently a Research Scientist with Honeywell, Inc., Broomfield, CO, USA, where he is involved in photonics technology and process development and optical system design. He was a Graduate Student Researcher with the Optical Communications and Photonic Integration Group, UCSB, where he investigated low-noise on-chip waveguide lasers and ultralow-loss waveguide delays for sensing applications.

**Taran A. Huffman** received the B.S. degree in physics from the University of Southern California, Los Angeles, CA, USA. He is currently working toward the Ph.D. degree with the University of California, Santa Barbara (UCSB), Santa Barbara, CA. Since 2012, he has been a Graduate Student Researcher at UCSB. His research interests include the design and fabrication of low-loss waveguides on the SiN platform. Much of his work involves resonators, but he is also developing a method for vertically integrating waveguide layers.

**Minh A. Tran** (S'14) received the B.S. degree in electrical engineering from the University of Tokyo, Tokyo, Japan, in 2013, and the master's degree in 2015 from the University of California, Santa Barbara, CA, USA, where he is currently working toward the Ph.D. degree in electrical engineering. His research interests include ultralow-loss waveguides, low-noise high-power lasers and photonics-integrated circuits.

**Tin Komljenovic** received the M.Sc. and Ph.D. degrees in electrical engineering from the Faculty of Electrical Engineering and Computing, University of Zagreb, Zagreb, Croatia, in 2007 and 2012, respectively. During his Ph.D. studies, he was a Visiting Researcher with IETR, University of Rennes. He is currently a Research Scientist with the University of California Santa Barbara, Santa Barbara, CA, USA, where his research focuses on photonic integration. He has authored or coauthored more than 60 papers and seven patents. His current research interests include integrated photonic circuits, tunable optical sources, and LIDAR. He received the EuMA Young Scientist Prize and the Marie Curie FP7 grant.

**John E. Bowers** (F'94) received the M.S. and Ph.D. degrees from Stanford University, Stanford, CA, USA. He is the Director of the Institute for Energy Efficiency and a Professor in the Departments of Electrical and Computer Engineering and Materials, University of California, Santa Barbara (UCSB), Santa Barbara, CA. His research interests are primarily concerned with silicon photonics, optoelectronic devices, optical switching and transparent optical networks, and quantum dot lasers. He worked for AT&T Bell Laboratories and Honeywell before joining UCSB. He is a Fellow of the Optical Society of America (OSA) and the American Physical Society. He has received the IEEE Photonics Award, the OSA/IEEE Tyndall Award, the IEEE LEOS William Streifer Award, and the South Coast Business and Technology Entrepreneur of the Year Award. He is a member of the National Academy of Engineering and the National Academy of Inventors.

**Daniel J. Blumenthal** received the Ph.D. degree from the University of Colorado, Boulder, CO, USA. He is currently a Professor in the Department of Electrical and Computer Engineering, University of California, Santa Barbara, CA, USA, where he is the Director of the Terabit Optical Ethernet Center and heads the Optical Communications and Photonics Integration group. He is the co-Founder of Packet Photonics and Calient Networks, startups for Telecommunications and Data-Communications. He holds 21 patents, has authored or coauthored more than 410 papers in the areas of optical communications, optical networks and packet switching, optical gyro sensors, photonic integration in InP, SiPh/InP and ultralow-loss waveguide platforms, and silicon photonic and nanophotonic device technologies. He coauthored the book entitled *Tunable Laser Diodes and Related Optical Sources* (New York, NY, USA: IEEE Press–Wiley, 2005). He is a Fellow of the IEEE Lasers and Electro-Optics Society and the Optical Society of America. He has served on the Board of Directors for National LambdaRail and as an elected member of the Internet2 Architecture Advisory Council. He has received a Presidential Early Career Award for Scientists and Engineers, a National Science Foundation Young Investigator Award, and a Office of Naval Research Young Investigator Program Award.